X-ray absorption fine structure and magnetization characterization of the metallic Co component in Co-doped ZnO thin films

Steve M. Heald
Argonne National Laboratory, Argonne, Illinois 60439, USA

Tiffany Kaspar, Tim Droubay, V. Shutthanandan, and Scott Chambers
Pacific Northwest National Laboratory, Richland, Washington 99352, USA

Abbas Mokhtari, Anthony J. Behan, Harry J. Blythe, James R. Neal, A. Mark Fox, and Gillian A. Gehring
Department of Physics and Astronomy, University of Sheffield, Sheffield S3 7RH, United Kingdom
(Received 26 August 2008; revised manuscript received 16 December 2008; published 4 February 2009)

X-ray absorption fine-structure (XAFS) measurements have been used to characterize a series of Co-doped ZnO films grown on sapphire substrates by pulsed laser deposition. The emphasis is on characterization of the fate of the Co dopant: metallic particles or substitutional Co2+. It is shown that analysis of both the near edge and extended fine structure can provide a measurement of the fraction of metallic Co. Any quantitative understanding of magnetism in this system needs to take into account both types of Co. Results are reported for two types of films from two different groups that show distinctly different behaviors. Films grown with high concentrations of Co show varying amounts of metallic Co that could be identified as a close-packed form of Co. Another set of films was annealed in Zn vapor to induce magnetism. These films also showed significant metallic Co, but of a different type similar to the CoZn intermetallic. The bulk forms of both metals are magnetic and should contribute to the magnetism. However, the measured room-temperature magnetic moments for some films are inconsistent with the expected moments based on the bulk magnetic values for either Co metal or CoZn. The magnetic properties of the small metal particles are likely changed by their surroundings. Low-temperature magnetic measurements for one of the samples confirmed this with an estimated blocking temperature of 50 K.

DOI: 10.1103/PhysRevB.79.075202 PACS number(s): 78.70.Dm, 75.50.Pp

I. INTRODUCTION

Co-doped ZnO has been widely investigated as a dilute magnetic semiconductor (DMS) which may potentially exhibit room-temperature ferromagnetism, but disparate experimental results have prevented consensus on the existence and mechanism of intrinsic ferromagnetism.[1–4] In several reports involving careful material characterization, the observed ferromagnetism has been shown to arise from ferromagnetic secondary phases,[5–9] leading to speculation that undetected inclusions have generated spurious magnetic signals in other less well-characterized materials.[1,4] Furthermore, well-characterized single-phase material that does not exhibit intrinsic ferromagnetism has been reported.[10,11] On the other hand, measurements of magnetic moments[12–14] have been reported that are in excess of what could occur if the magnetization arises solely from metallic cobalt, and particularly large moments have been observed in samples that were codoped with aluminum.[15–17] One possible explanation for this uncertainty and disagreement is that oxide magnetism seems to depend on defects for its existence. Here we define oxide magnetism as the intrinsic magnetism arising from Co substitution in ZnO. It is difficult to reproduce the same level of defects from one sample to another, and the most perfect films are nonmagnetic.[18]

For Co as a magnetic dopant, the principal impurity phase of concern is metallic Co. Cobalt metal is strongly ferromagnetic ($1.72\mu_B$/Co and T_c=1388 K), and can lead to spurious room-temperature ferromagnetic signals that may mimic those expected for an oxide DMS, although when metallic Co is in small superparamagnetic clusters there is no coercive field. When the clusters are blocked the coercive field is relatively high (~400 Oe), and thus magnetic characterization as a function of temperature is also needed. The presence of metallic Co must therefore be carefully considered and characterized both structurally and magnetically before claims of intrinsic ferromagnetism can be made. However, conventional material characterization techniques do not have the sensitivity to detect trace amounts of secondary-phase formation. X-ray diffraction (XRD) is commonly applied to investigate the phase purity of oxide DMS, but especially when using Cu $K\alpha$ x rays, it has been shown to have low sensitivity for Co metal.[19,20] Transmission electron microscopy (TEM) has the resolution to detect nanometer-sized inclusions, but the very small volume sampled by TEM may not be sufficient to detect highly disperse precipitates. For this reason, we have chosen to investigate the phase purity of Co:ZnO films by x-ray absorption fine structure (XAFS) studies.

XAFS measurements at the K edge are very useful for determining the valence state and local structure of Co in doped oxide systems.[10,11,21–23] In particular, since long-range crystalline order is not needed, XAFS can see the Co metal components even if they are disordered or in small nanoparticles.[6,24–26] Furthermore, both the near-edge region (XANES) and the extended fine structure (EXAFS) can be used to look for metallic components. For Co there is a large shift in energy going from the metal to the typical Co(II)

TABLE I. Properties of the samples studied. The measured Co concentrations are from PIXE measurements, and are defined as the fraction of Zn sites that contain Co. Magnetization and resistivity for samples P-1, P-2, and P-3 were measured after Zn diffusion treatment.

Sample ID	Deposition and substrate	Source dopant concentration	Measured Co concentration	Substrate T (°C)	O_2 pressure (mTorr)	Treatment	Thickness (nm)	Resistivity (Ω cm)	RT magnetization
P-1	Off-axis PLD c-Al_2O_3	0.04 Co	0.04	550	10	Zn vapor	7	0.03	$\sim 0.7\mu_B$/Co [a]
P-2	Off-axis PLD c-Al_2O_3	0.1 Co	0.16	475	10	Zn vapor	100	0.1	$0.03\mu_B$/Co
P-3	Off-axis PLD r-Al_2O_3	0.1 Co	0.16	475	10	Zn vapor	100	0.5	$0.04\mu_B$/Co
S-1	On-axis PLD c-Al_2O_3	0.05Co+0.006Al	0.26	450	10		80	0.095	~ 0
S-2	On-axis PLD c-Al_2O_3	0.05Co	0.09	450	10		50	0.15	$0.44\mu_B$/Co
S-3	On-axis PLD c-Al_2O_3	0.05Co+0.015Al	0.17	450	0.05		240	0.0018	$0.23\mu_B$/Co
S-4	On-axis PLD c-Al_2O_3	0.05Co+0.006Al	0.25	450	10		170	0.0015	$0.1\mu_B$/Co

[a]The room-temperature saturation magnetization for this film (3×10^{-6} emu) was at the sensitivity limit of the VSM.

valence. Similarly the metallic Co near-neighbor bond length is quite different from those in ZnO, falling between the Zn-O and Zn-Zn first- and second-neighbor bond lengths. Both measurements have sensitivity to a few percent of the Co atoms forming metallic bonds.

In this paper we report XAFS studies on Co:ZnO samples from two laboratories that exhibit a range of magnetic moments measured at room temperature. The XAFS results that we present here lead us to conclude that most of the Co-doped ZnO films investigated contain at least some metallic Co. The fraction of Co in the metallic phase varies widely from sample to sample, and two distinct types of metallic Co are found, one phase similar to Co metal [hexagonal-closed packed (hcp) or face-centered cubic (fcc)] and a second phase similar to CoZn intermetallic.[6] In one sample the orientation dependence of the EXAFS indicates the CoZn metallic phase is oriented with respect to the ZnO lattice. These results demonstrate the power of XAFS methods in characterizing DMS materials.

II. EXPERIMENTAL

A. Sample preparation

Information on the samples reported in this paper is summarized in Table I. Samples P-1 to P-3 were grown at Pacific Northwest National Laboratory (PNNL), and samples S-1 to S-4 were grown at the University of Sheffield.

Samples P-1 to P-3 were deposited using pulsed laser deposition (PLD) in an off-axis PLD configuration, utilizing a KrF excimer laser ($\lambda=248$ nm) at 1–5 Hz with an energy density of ~ 2.4 J/cm^2 incident on the target. Co-doped ZnO epitaxial thin films were deposited on single crystal c-plane $Al_2O_3(0001)$ and r-plane $Al_2O_3(1\text{-}102)$ substrates. Depositions were performed at a substrate temperature of 475–550 °C in 10 mTorr O_2; the deposition rate was approximately 0.25 Å/laser pulse. Further details of the deposition process have been given elsewhere.[11] For the as-deposited films, XANES and EXAFS measurements identical to those described here indicated a lack of Co(0) within the detection limit (estimated as 3–5% of the total Co content), and the films exhibited no ferromagnetism.[11]

To induce room-temperature ferromagnetism in Co:ZnO, samples P-1 to P-3 were annealed in Zn vapor at 600 °C for 5 h. After this treatment, n-type conductivity and weak room-temperature ferromagnetism were observed as discussed previously.[6] For the samples discussed here, a significant fraction of Co(II) was reduced to Co(0) during the Zn vapor treatment, resulting in clear detection by XAFS. The film thickness was measured by x-ray reflectivity and/or Rutherford backscattering spectrometry. Composition was measured by proton-induced x-ray emission (PIXE). The magnetization was measured at room temperature by vibrating sample magnetometry (VSM), with the field applied in the plane of the film. After the XAFS measurements, the magnetization was confirmed using the Sheffield superconducting quantum interference device (SQUID) magnetometer, except for the very thin sample P-1 that appeared to have been contaminated. The resistivity was determined by a four-point probe at room temperature.

The samples from Sheffield (S-1 to S-4) were chosen since they exhibit different magnetizations (including S-1 that was nonmagnetic at room temperature), contain different amounts of Al dopant, and were deposited at different oxygen pressures. The stoichiometric targets of composition $Zn_{1-x-y}Al_xCo_yO$ with $y=0.05$ were prepared by mixing appropriate amounts of 99.999% pure ZnO, Co_3O_4, and Al_2O_3 with subsequent grinding for about 15 min. The powders of Co- and Al-codoped ZnO were fired at a temperature of 400 °C and the pressed pellet was calcined at 400 °C for 8 h. The resulting pellets were used as targets in a PLD chamber, where they were ablated, in an on-axis configuration, using a Lambda Physik XeCl laser ($\lambda=308$ nm) at a repetition rate of 10 Hz. During deposition, the partial oxygen pressure was held constant at a value above the base pressure (3×10^{-5} Torr) as shown in Table I. The films, with thickness varying from 50 to 240 nm, were grown on c-plane (0001) sapphire substrates. During film deposition, the substrate temperature was held at 450 °C. The sample thickness was measured using a Dektak profilometer; magnetization measurements were carried out in a Quantum Design SQUID magnetometer; and Hall-effect measurements were made in a continuous-flow cryostat equipped with an iron core magnet. The concentration of Co in the deposited films was measured by PIXE at PNNL. The quoted magnetizations per Co atom

were determined using the measured concentrations. Due to the Al_2O_3 substrates, the final concentration of Al in the samples could not be determined.

B. XAFS measurements

The XAFS measurements were made at Sector 20 at the Advanced Photon Source (APS) using beamlines 20-BM and 20-ID.[27] Both beamlines use Si (111) monochromators that give an energy resolution close to the Si (111) limit of $\Delta E/E = 1.3 \times 10^{-4}$. On 20-BM, measurements were made with the x-ray polarization parallel to the surface of the films. A combination harmonic rejection/focusing mirror focused the beam vertically to about 20 μm. The sample angle was adjusted for glancing incidence (a few degrees off the surface) to enhance the signal while still probing the entire thickness. For all measurements the samples were spun at a few hertz about the surface normal to minimize interference from substrate and film Bragg peaks. On 20-ID the microprobe station was used to provide a focused beam size of 2–5 μm. This allowed glancing angle measurements with the polarization both parallel and perpendicular to the surface of the films. On both beamlines a multielement Ge detector was used to select the Co fluorescence for counting. The combination of spinning and an energy resolving detector completely eliminated any interference from Bragg peaks. Co metal and CoZn standards were measured in transmission for a thin foil and fine powder on Kapton tape, respectively. The Co metal sample was also used as an online reference for all measurements to check the monochromator energy calibration. Its edge position (maximum in the first derivative) was taken as 7708.8 eV.[28]

On both beamlines multiple scans (five to ten) were made to achieve a Co fluorescence count of several million at the end of the EXAFS region. This gave high-quality data as shown in Figs. 1 and 2. In all cases the spectra had features that looked similar to the Zn site in ZnO, demonstrating that much of the Co is taking up substitutional sites. This is made clear in Fig. 3, which shows the Fourier transforms of some of the data. All of the data show the peaks characteristic of Co in a Zn site in ZnO. The amount of metallic Co as indicated by the central peak varies from 0% to nearly 40% of the Co. The presence of metal is also clearly seen in the near-edge region [Figs. 1(a) and 2(a)]. In this case the interpretation is complicated by the small peak present in metal-free Co substituted ZnO. This is due to 1*s*-to-3*d* transitions that become slightly allowed by the nearly tetrahedral bonding of Co at the Zn sites.

All of the data shown so far are for ZnO grown on *c*-plane Al_2O_3 substrates. In this case the films grow with the (0001) orientation, and the orientation dependence of the EXAFS was rather small. Sample P-3, *a*-plane ZnO(110) grown on *r*-plane Al_2O_3, showed much stronger orientation dependence. The transforms of these data are shown in Fig. 4. In this case there is a large amount of metal, but the metal peak shows a strong dependence on the x-ray polarization. This is not expected for Co metal that has an hcp structure. The presence of this dependence leads us to consider other possible metallic forms of Co. For EXAFS, fcc Co would look

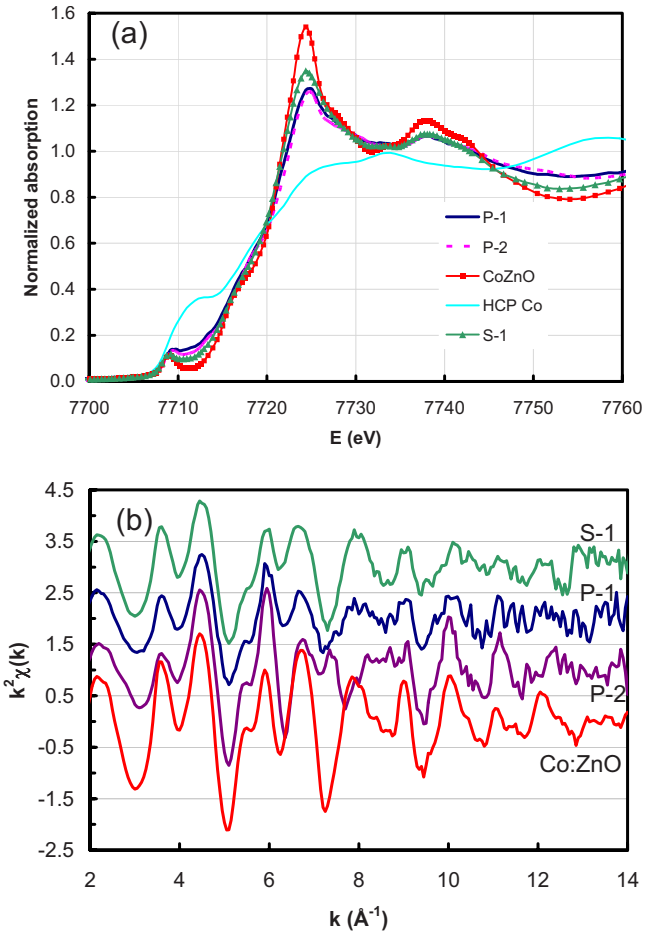

FIG. 1. (Color online) Some examples of data for the Co (a) near edge and (b) EXAFS from some Co-doped ZnO samples that had a significant metal component. The x-ray polarization is in the plane of the film. The data labeled Co:ZnO are an example of a metal-free spectrum.

essentially the same as hcp Co and cannot explain the difference. Another possibility is the CoZn intermetallic compound.[29–31] It has a structure with natural orientation dependence, and is also ferromagnetic with a substantial moment.[6] The transform of data from unoriented CoZn powder[32] is also shown in Fig. 4. Note that its peak lines up closely with the metal peak in the transform for sample P-3.

III. DATA ANALYSIS

A. Near-edge fitting

The data were analyzed using the Athena and Artemis interfaces to the IFEFFIT program package.[33] Theoretical calculations were done using FEFF 8.4.[34] The first step in the analysis was to use the near-edge spectra to estimate the amount of metal present. The simplest approach is to fit the near edge with a linear combination of the cobalt standards. A complication here is the choice of the proper standard. The height of the structure at the top of the edge seemed to vary by more than could be explained by the metal component. This could be due to differing disorder in the ZnO lattice for

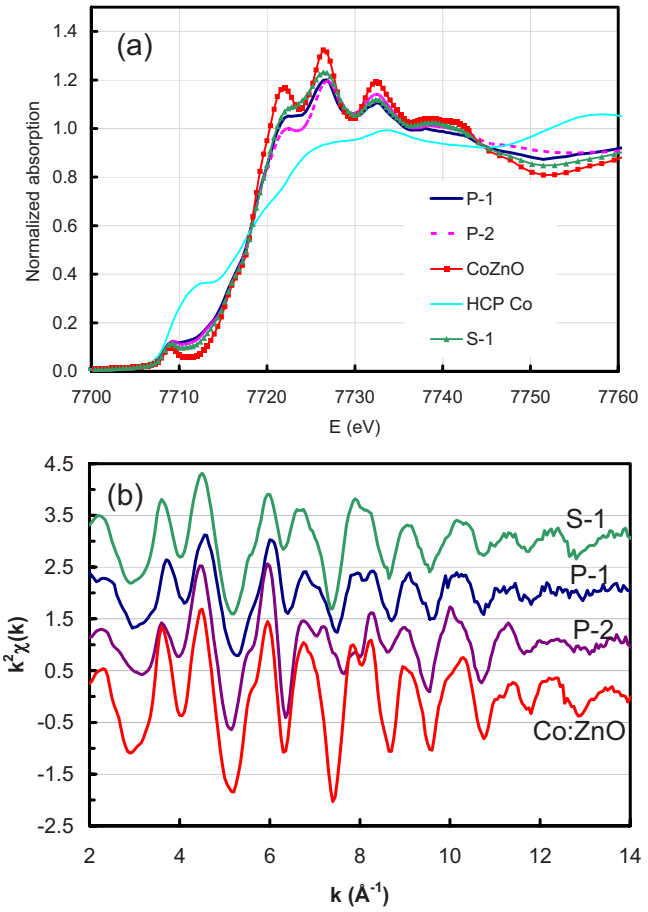

FIG. 2. (Color online) Data for the same samples as in Fig. 1 with the x-ray polarization perpendicular to the plane of the film.

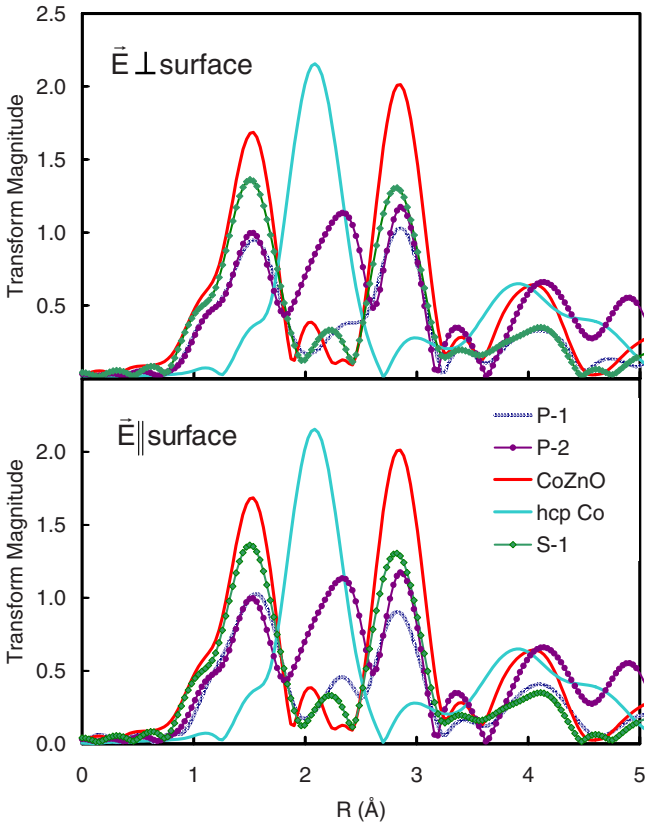

FIG. 3. (Color online) Fourier transforms of the data in Figs. 1(b) and 2(b) showing the location of the metallic bonds between the first and second shells of ZnO for the two x-ray polarization directions. The transform range is 2–12 Å^{-1} with k^3 weighting. For clarity, the Co metal transform has been divided by 2.

the different samples. Therefore, the fits were carried out for just the lower half of the edge, which is more sensitive to the valence and less sensitive to other structural distortions. Then the choice of standard becomes less important for the substitutional Co in ZnO spectrum. There is still the choice of Co or CoZn metal for the metal standard. In the case of CoZn there could be an orientation dependence to the edge as was observed in the EXAFS data for one of the samples. Since the CoZn standard was only measured in powder form, the near-edge fitting for the samples was carried out on the powder-averaged data. For thin-film samples this is 1/3 of the perpendicular orientation signal plus 2/3 of the parallel orientation signal.[35] The results are shown in Table II, and some examples are given in Fig. 5. Also shown in Table II is the *r* factor, which gives a measure of the fit quality. Comparing the Co and CoZn fits shows that the Co standard often gives slightly better fits, but the differences are usually barely significant. EXAFS analysis can better distinguish between the two types of metals.

B. EXAFS analysis

1. Comparison of the metal signals

Before carrying out detailed fitting of the EXAFS data, it is instructive to try to isolate the metal component by subtracting out the substitutional (ZnO) component. This allows the metal component to be examined without significant interference from the neighboring peaks. Figure 6 shows two examples for cases with a large metal component. To generate these, the amount of subtracted Co:ZnO was varied until

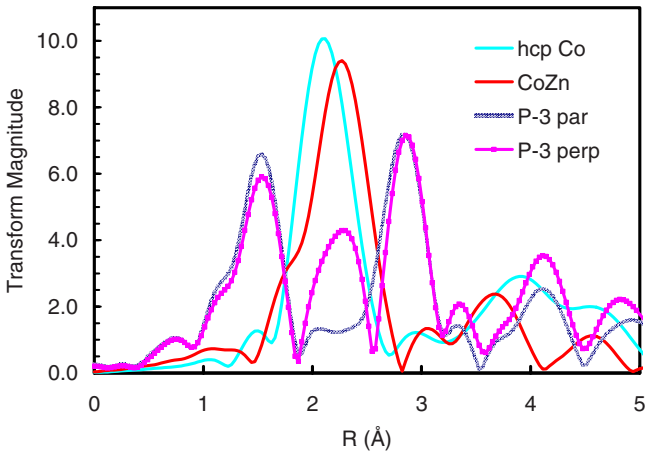

FIG. 4. (Color online) Fourier transforms of the data from the Co-doped ZnO sample that showed substantial orientation dependence. The transform range is 2–12 Å^{-1} with k^3 weighting. For comparison, similar transforms are included for data from Co metal (divided by 3) and unoriented CoZn powder.

TABLE II. Percentage of added Co that has Co(0) valence (metallic) and has Co(2+) valence characteristic of substitutional sites in ZnO. These are determined from fits to the lower part of the near edge for powder-averaged data. Results using both Co metal and CoZn standards for Co(0) are compared using the *R* factor in the ATHENA program as a measure of the fit quality. The fitting errors were typically about 1%. Systematic errors contribute another 1–2% error in these values. Therefore the values of less than 3% are consistent with 0.

	Percentage Co(0) as Co metal	Percentage Co(2+) in ZnO site	*R* factor	Percentage Co(0) as CoZn	Percentage Co(2+) in ZnO site	*R* factor
P-1	31	69	0.00034	25	75	0.00038
P-2	28	82	0.00150	23	77	0.00160
P-3	16	84	0.00059	12	88	0.00091
S-1	17	83	0.00012	14	86	0.00030
S-2	7	93	0.00012	5	95	0.00017
S-3	4	96	0.00059	3	97	0.00065
S-4	1	99	0.00078	1	99	0.00079

the ZnO peaks were minimized. The subtracted amount needed was less than the near-edge fits indicated, suggesting that there is even more metal present. However, these values may also indicate that the amount of disorder in the ZnO lattice is changing. It is likely that metallic inclusions increase the disorder, reducing the ZnO signal in samples that contain metal. Therefore, the near-edge derived concentration values were used for normalizing the signal of the subtracted metallic component signal.

For comparison, data from hcp Co metal are also plotted in Fig. 6(a). This comparison indicates that for S-1 the metallic component is essentially identical to hcp Co metal even for the more distant shells. Examination of the normalized EXAFS [χ(k)] data indicates that most of the amplitude difference can be explained by disorder giving a larger Debye-Waller (σ^2) factor.

For the Zn-annealed sample P-2, the situation is not as clear. The larger metal concentration seems to distort the ZnO lattice more strongly, and the subtraction is not as clean, especially for larger distances. However, in Fig. 6(b) the main isolated peak lines up closely to the Co-Zn shell in CoZn. This is additional evidence that both types of metal bonding need to be considered when fitting the data.

Since there is Al in some of the samples as well as Al in the substrate, Co-Al compounds are also a possibility that was considered. However, comparison of a possible Co-Al signal with the isolated metal signals in Fig. 6 rules out significant Co-Al bonding. The Al EXAFS is shifted in phase by approximately π, and has much different *k* dependence. The bond parameters in possible intermetallic compounds

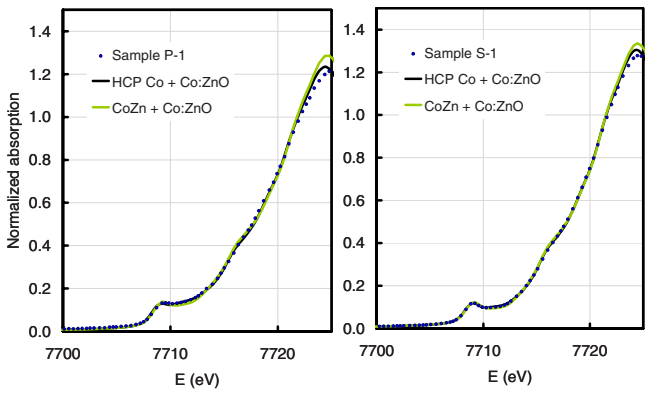

FIG. 5. (Color online) Examples of the near-edge fitting for two samples with a significant metallic component. The points are the measured data, and fits using hcp Co and CoZn for the metal component are compared. The fitting range was 7700–7721 eV.

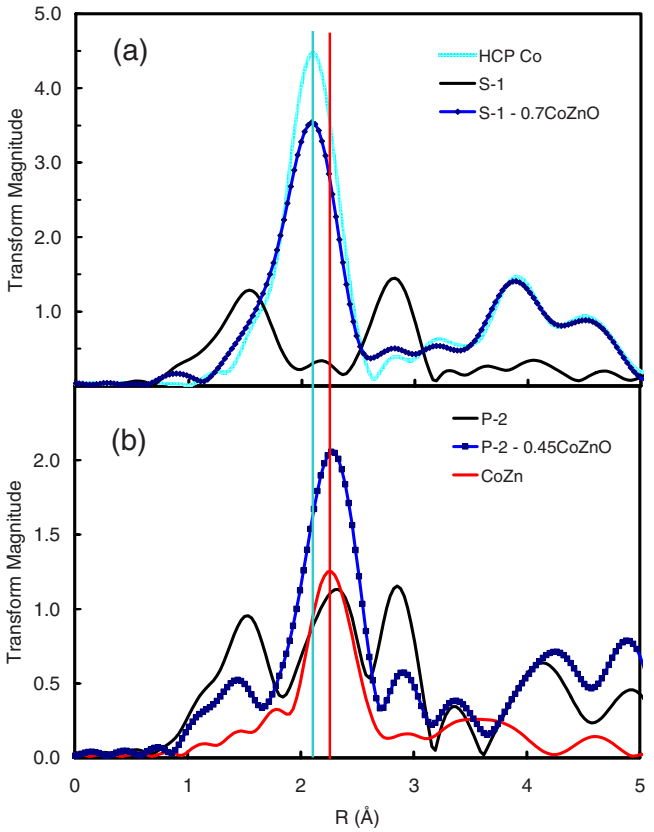

FIG. 6. (Color online) Fourier transforms of the results of isolating the metal component by subtracting the Co:ZnO signal for samples (a) S-1 and (b) P-2. Included for comparison are the Co metal (divided by 2) and CoZn spectra.

such as CoAl would have to be severely distorted to obtain an even approximate match to the data. Even Co-rich compounds such as Co_3Al have significant Co-Al bonding at short distances that causes a mismatch with the measured data.

2. CoZn and the orientation dependence

Both of the samples in Fig. 6 are Co:ZnO(001) on *c*-plane substrates; no polarization dependence of the metallic signal is observed. In Fig. 4 the metallic Co peak for a sample grown on an *r*-plane substrate is clearly seen to line up with the CoZn peak even without subtraction of the ZnO peaks. In this case, however, there is a large polarization dependence with the peak much reduced when the polarization is in the plane of the film.

The x-ray signal derives from bonds aligned with the x-ray polarization. The signal varies as the $\cos^2$ of the angle between the bond direction and the polarization vector. Thus we need to consider the structure of the possible metals. Pure Co typically has the hcp structure with a nearly symmetric arrangement of 12 near-neighbor atoms. The fcc structure is also a possibility for pure Co, and it would also have a symmetric arrangement of near neighbors. The hcp and fcc Co structures cannot be distinguished by EXAFS since they have almost identical near-neighbor environments. For both structures no orientation dependence would be expected for the first shell of bulk Co. However, if the Co particles were small enough and asymmetrically shaped, there could be an orientation-dependent amplitude due to variation in the average number of neighbors. For example, if the metallic particles were thin (a few atomic layers) platelets oriented in the plane of the film, the signal from Co-Co bonds would be stronger for the polarization in the plane of the film.

Oriented CoZn will have an orientation dependence even if the particles are symmetric. The complete structure of CoZn has not been reported. It has been determined to be in the β-Mn structure with the 8*c* sites fully occupied by Co and Zn in the 12*d* sites.[29–31] For stoichiometry 1/6 of the 12*d* sites must be Co. However, these references did not provide the detailed atomic coordinates. Figure 7 shows the near-neighbor environment around an 8*c* Co atom in CoZn assuming that the atomic coordinates are the same as for β-Mn. The near-neighbor distances are listed in Table III. The first shell EXAFS signal is determined by two distances, one at 2.36 Å and an average shell near 2.62 Å. For the EXAFS signal the backscattering from Co and Zn are similar. Therefore, a Co in a 12*d* site would have a signal similar to the longer distances in the 8*c* site. The ratio of these two contributions varies strongly with x-ray polarization. When the polarization is in the plane formed by the three Co neighbors, the contribution from the short and long distances is similar. Perpendicular to this plane, only the long distance will contribute.

Fitting to the CoZn powder, Co EXAFS data gave slightly shorter distances than predicted above, as shown in Table III. In these fits it was assumed that the Zn neighbors had three distances with the same spread as for the calculated structure. The resulting common Debye-Waller factor for these neighbors was fairly large (0.0105), suggesting that the real spread

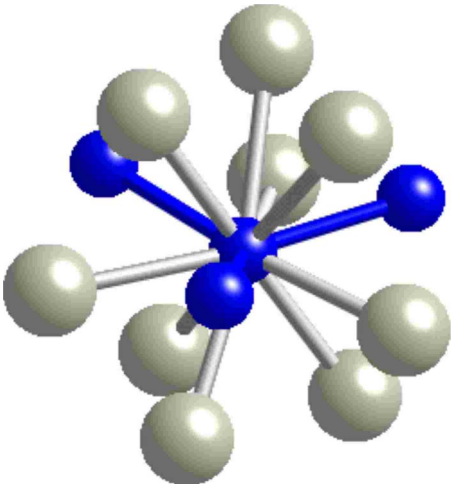

FIG. 7. (Color online) The atomic arrangement around an 8*c* Co site in CoZn. The Co atoms are smaller (blue).

is probably somewhat larger. Also, if the occupancy of the Co 8*c* site was allowed to vary, the fits tended to converge to a reduced occupancy, suggesting some of the 8*c* sites could be filled with Zn atoms. However, these refinements have little effect on the results presented below for the Co:ZnO samples, and for all of the fits it is assumed that the 8*c* sites are fully occupied by Co.

3. Fitting results

Before starting the fitting, one more piece of information is available from the *r*-plane data. Figure 8 shows the result of isolating the metal signal in Fig. 4 by using the inverse transform over the region 1.8–2–6 Å. We see that both polarizations have a metal signal. The apparent loss of the peak for the parallel case is due to a beating between two different

TABLE III. Near-neighbor environments for the 8*c* and 12*d* sites in CoZn. The 8*c* sites are Co and the 12*d* sites are mostly Zn. The measured results are from fitting the EXAFS from CoZn powder. In these fits it was assumed that the three Zn distances had the same spread of distances as for the calculation.

Neighbor type	*N*	Distance (Å)	Measured distance (Å)
		8*c* site	
Co	3	2.36	2.34
Zn	3	2.57	2.54
Zn	3	2.63	2.60
Zn	3	2.67	2.64
		12*d* site	
Co	2	2.57	
Co	2	2.62	
Zn	4	2.64	
Zn	2	2.67	
Co	2	2.67	

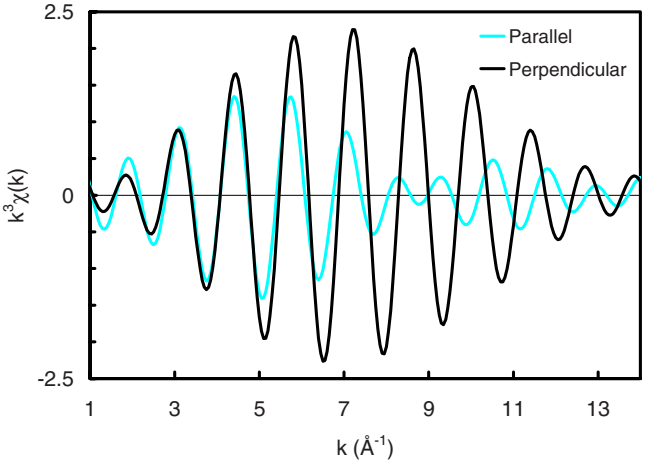

FIG. 8. (Color online) Inverse transform of the data in Fig. 4 over the range 1.8–2.6 Å for the *r*-plane parallel and perpendicular data.

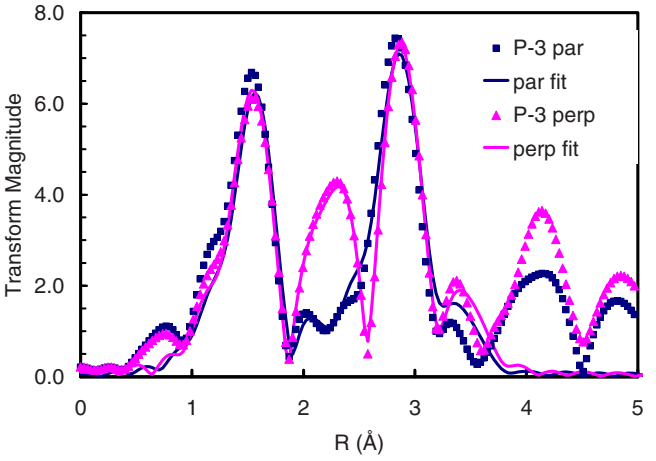

FIG. 9. (Color online) Fit to the *r*-plane data using a model of oriented CoZn and Co in ZnO.

distances. This is expected for CoZn. However, the beating has a minimum near $k=9$ Å^{-1}. This suggests the two distances are separated by about 0.17 Å, which is less than the observed difference between the two shells in CoZn (an average of 0.26). Therefore, we have to consider the possibility that the oriented CoZn is distorted by its epitaxial relationship with the ZnO lattice.

The results of fitting the *r*-plane sample are shown in Fig. 9 and Table IV. For this fit the data from the two polarizations were fitted simultaneously with many parameters in common. On *r*-plane substrates, ZnO grows in the (110) orientation. As discussed above, to minimize Bragg-peak interference the sample was spun about the surface normal. Therefore, when the x-ray polarization is perpendicular to the surface it is measuring a pure (110) orientation. When the polarization is in the plane of the film (parallel polarization) the EXAFS is an equal mixture of (001) and (1-10) orientations. These orientations were assumed in the FEFF calculations for ZnO. For CoZn the observed orientation dependence requires it to be oriented with its (111) lattice direction along the ZnO (110).

Once the orientation is established, the fitting model is highly constrained. For ZnO, the fit included the first four Zn-O and Zn-Zn shells, contributing to the two main transform peaks. For these shells separate Debye-Waller factors (σ^2) were used, but for the distances only a single overall lattice-parameter correction was used. For CoZn a common Debye-Waller factor and Δr were used for the three Co-Zn distances, and both were allowed to vary for the short Co-Co distance. The amplitude factor S_0^2 was fixed at 0.8 as determined by fitting Co metal and other Co oxide standards. The other fitting parameters were E_0 and the fraction of CoZn. The fitting range for the two files was 2–12.5 Å^{-1} in *k* space and 1–3.5 Å in *r* space, giving 32 independent points, while the model only had 11 fitting parameters.

This highly constrained model gave a good fit to the data with parameters that seem reasonable (Table IV). The orientation dependence is accurately reproduced. The disorder in the ZnO is increased as might be expected when an impurity phase is present. The amount of CoZn is significantly larger than that determined by the near-edge fitting. Also, the Co-Co bond length (2.55 Å) has increased significantly from the CoZn powder result (2.36 Å, Table III), as expected from the previous back transform analysis of the metal signal (Fig. 8).

For the fitting of the *c*-plane samples the polarization dependence is different. The ZnO grows in the (001) orientation, so the perpendicular polarization data is pure (001). For the parallel polarization, the spinning means the signal can

TABLE IV. Fitting parameters for the *r*-plane fit shown in Fig. 9 and described in the text. The fit refined to 75 ± 4% of the Co in ZnO sites and 25 ± 4% in the form of CoZn. The results for a similar fit on a Co:ZnO sample with no metal are listed for comparison. In that case the fit refined to 0% CoZn as expected.

			Sample P-3		Co:ZnO	
	Neighbor	N[a]	R	σ^2	R	σ^2
ZnO	O	4	1.97 (0.01)	0.0046 (0.001)	1.97 (0.01)	0.0028 (0.001)
	Zn	12	3.21 (0.01)	0.0104 (0.001)	3.21 (0.01)	0.0078 (0.001)
	O	8	3.80 (0.02)	0.0041 (0.003)	3.80 (0.02)	0.0056 (0.003)
CoZn	Co	3	2.55 (0.03)	0.0094 (0.003)		
	Zn	9	2.68 (0.02)[b]	0.0083 (0.002)		

[a]Fixed values.
[b]Average of three similar distances.

TABLE V. Fitting results for the *c*-plane sample P-2 using a model with Co:ZnO and CoZn.

	Neighbor	N^a	R	σ^2
ZnO (72 ± 5%)	O	4	1.97 (0.01)	0.0059 (0.001)
	Zn	12	3.21 (0.01)	0.0091 (0.001)
	O	8	3.80 (0.02)	0.0010 (0.003)
CoZn (28 ± 5%)	Co	3	2.56 (0.03)	0.0010 (0.004)
	Zn	9	2.67 (0.02)[b]	0.0026 (0.002)

[a]Fixed values.
[b]Average of three similar distances.

be considered on average as (110) oriented ZnO. In this case, if the CoZn is still aligned with its (111) along the ZnO (110), the spinning would average the signal to give smaller orientation dependence. For this orientation the *c*-plane perpendicular data should look like the *r*-plane parallel data with the beating behavior reducing the amplitude. This is not observed. Therefore, it appears that while CoZn is present in the *c*-plane samples, it is not oriented. For the *c*-plane fits we have assumed unoriented CoZn metal signals. The fit result is shown in Table V.

For unoriented CoZn the signal is dominated by the signal from the long Co-Zn bonds. This means the fits are not very sensitive to the Co-Co contribution. The same fits were tried with hcp Co metal. In this case the Co-Co distance refined to the same value as the Co-Zn distance, and the other values were also similar. This is expected since the EXAFS from Co-Co and Co-Zn bonds is very similar and in either case, the metallic component is dominated by a single shell. The main reason to prefer CoZn in this case is the large bond distance. It is possible the Co metal is being distorted by the ZnO lattice, but having the same large distortion in both polarization directions seems less likely.

This conclusion is further strengthened when the data from the *c*-plane sample S-1 are analyzed in detail. These fit results are shown in Table VI. Although the results in Fig. 6(a) strongly indicate Co metal, both cases were considered in the fitting. Again both the Co metal and CoZn fits were of similar quality and had similar values. In this case the metal-metal distance is more similar to Co metal, and actually refined to a slightly smaller distance than the bulk metal. It seems unlikely that the same Co metal particles would be slightly compressed in one case and highly expanded in the other since the matrix is the same. Therefore, we conclude that we have two types of metal present in these samples, Co metal (hcp or fcc) and another with bonding similar to CoZn.

TABLE VI. Fitting results for the *c*-plane sample S-1 using a model with Co:ZnO and Co metal.

	Neighbor	N^a	R	σ^2
ZnO (85 ± 4%)	O	4	1.97 (0.01)	0.0041 (0.001)
	Zn	12	3.21 (0.01)	0.0104 (0.001)
	O	8	3.80 (0.02)	0.0085 (0.003)
Co (15 ± 4%)	Co	12	2.48 (0.03)	0.011 (0.003)

[a]Fixed values.

The other Sheffield samples had low levels of Co that were difficult to fit quantitatively. A fit to sample S-2 gave parameters for Co-Co bonding consistent with S-1 and refined to 7–10% Co metal. This is consistent with the near-edge fitting.

IV. CORRELATION WITH MAGNETIC PROPERTIES

The XAFS results reported in Sec. IV establish that the metallic phase is most likely to be CoZn in the PNNL samples and to be close-packed Co metal in the Sheffield samples. Here we present a brief summary of the conclusions that can be drawn from a comparison of the compositional analyses and the known magnetic moments measured at room temperature, and the temperature-dependent study made of sample S-1. Sample S-1 is particularly interesting because it was found to have the highest fraction of metallic Co of all the Sheffield samples, but was not ferromagnetic at room temperature although hysteretic magnetism occurred below 50 K. Therefore, it was investigated most carefully in this study. Room-temperature magnetic measurements are not a complete characterization, and we shall present detailed results that correlate the structural analysis by XAFS with the temperature dependence of the magnetic properties of the other samples that were magnetic at room temperature in another publication.

Table VII compares the magnetization expected for the metallic phase with the experimental values measured at room temperature. Some of the samples had high fractions of Co in a metallic form: P-2, P-3, and S-1. These samples are notable for having the lowest magnetization at room temperature. Indeed it was considerably *lower* than that expected from the metallic Co (the magnetization measurements on P-1 were not reliable because it was so thin). It may be that this occurs because the clusters are sufficiently small that they are not blocked at room temperature; a study of Co nanoparticles in ZnO has shown that the particles are blocked at 300 K provided that their radius is greater than about 8 nm,[36] which sets an upper limit to the cluster size. Another explanation is that the clusters are shaped such that many of the Co atoms at the edge have other Co atoms with which they can form antiferromagnetic bonds by superexchange through intervening oxygen.

Sample S-1 is interesting because the metallic component was positively identified as close-packed cobalt, which has a high anisotropy and gives rise to high coercive fields characteristic of blocked particles at low temperatures. This is in contrast to CoZn, which has a much lower anisotropy and thus cannot be identified by a change in coercive field alone. In Fig. 10 we show hysteresis loops at 100 and 5 K. At 100 K the coercive field is ~30 Oe, which is below the value of ~100 Oe normally recorded for an oxide film,[2,37] and so the film should be regarded as superparamagnetic at this temperature. However, at 5 K the coercive field has risen to 590 Oe, which is significantly *above* the value normally observed in oxide magnets, and is comparable to what might be expected for Co nanoparticles.[36] In addition, at low temperatures the ratio of remanence to saturation magnetization has risen to 0.42, which is approaching the value of 0.5 expected

TABLE VII. Comparison of the measured magnetization at room temperature with that expected from the metallic Co component assuming that the bulk moment is $1.72\mu_B$ for metallic Co and $1.35\mu_B$ for metallic CoZn. For close-packed Co the bulk magnetism is the same for the fcc and hcp phases (Ref. 43).

Sample	Percentage of cations that are Co	Fraction of Co atoms that are Co(0)	Expected magnetization due to metallic Co (μ_B/Co)	Measured RT magnetization (μ_B/Co)
P-2	16	0.28 CoZn	0.36	0.03
P-3	16	0.16 CoZn	0.22	0.04
S-1	26	0.17Co	0.29	~0
S-2	9	0.07 Co	0.12	0.44
S-3	17	0.04 Co	0.07	0.23
S-4	25	0.01 Co	0.02	0.10

for a random array of blocked particles. As shown in Fig. 11, the changes in the remanence and coercive field start to occur at about 50 K, which is an estimate for the blocking temperature. From other studies on blocked Co particles, we would estimate a cluster diameter of ~4 nm. The measured saturation moment at 5 K corresponds to $\sim 0.12\mu_B$/Co. This is still well below the $0.27\mu_B$/Co expected from the fraction of the Co (0.17) that is in the metallic phase, possibly due to antiferromagnetism as discussed earlier.

We now consider samples S-2, S-3, and S-4 that have metallic fractions of 0.07, 0.04, and 0.01, respectively. Given the uncertainty of the XAFS measurements, there is no firm evidence that there is *any* metallic Co in S-4, and the fraction in the other two samples is small. These samples are magnetic at room temperature and are similar to the samples on which MCD evidence for conduction-electron polarization has been published.[15,38] On balance the results support the conclusion that the films S-2, S-3, and S-4 show oxide magnetism as has been suggested.

V. DISCUSSION AND CONCLUSIONS

The conclusion that a close-packed form (hcp or fcc) of Co metal is present in the non-Zn-annealed sample with the highest metal concentration seems to be solid. There is good agreement between the isolated EXAFS and the standard even for the higher shells. The reduction in amplitude can be due to disorder or a particle size effect.[39–41] Particle sizes in the nanometer range will have a significant fraction of surface atoms that will likely be partially bonded to oxygen, reducing the metal-metal coordination number. For the fitting, the coordination was assumed to be the full value. A particle size effect would thus show up in the fits as a reduced percentage of metal and/or an increased Debye-Waller factor. The Debye-Waller factor for Co in sample S-1 is significantly larger than the bulk metal (0.011 compared to 0.0065). This could be due to being embedded in the ZnO lattice and/or a particle size effect not included in the fitting. Given the uncertainties in separating the disorder and amplitude effects on the weak metal signal, an attempt at determining the particle size from the EXAFS amplitudes does not seem warranted. However, for very small particles the higher shell amplitudes should be reduced more than the first shell amplitudes. Although the statistics for the higher shells are poor, and there could be interference from ZnO sites, they are visible at the expected distances. This seems to rule out very small particles of order 1 nm, consistent with the blocking temperature estimate of 4 nm. It was significant that the film that had the clearest evidence for metallic Co was not magnetic at RT, implying no oxide magnetism is present.

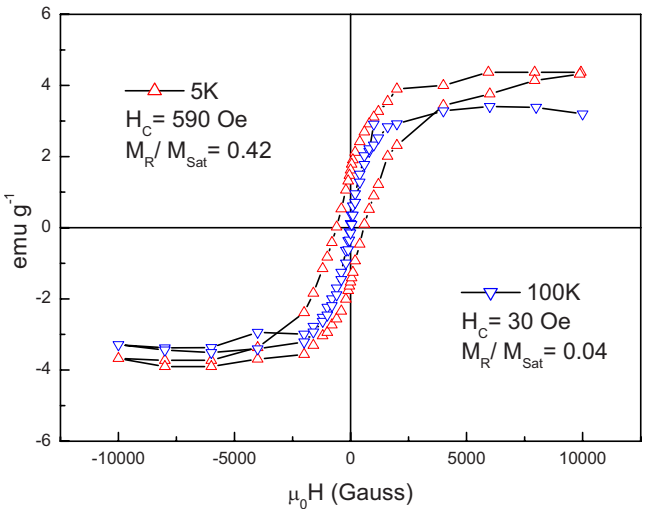

FIG. 10. (Color online) Hysteresis loops measured at 5 and 100 K for sample S-1.

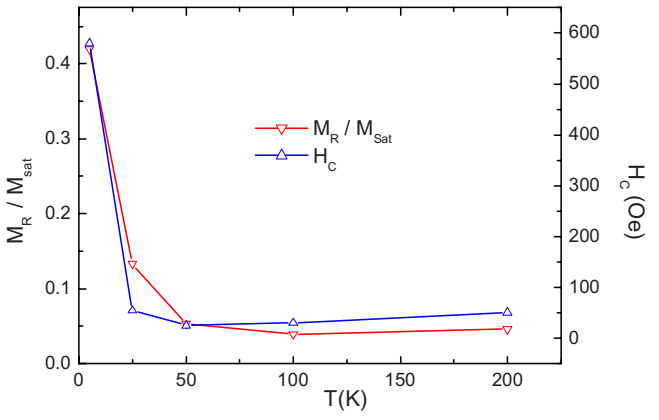

FIG. 11. (Color online) Temperature dependence of the coercivity and reduced remanence for sample S-1; data were obtained from full hysteresis loops performed at these temperatures.

However, this was expected because the carrier density of this film was such that previous studies indicated that it would not be ferromagnetic.[15]

The identification of a second form of metal in the Zn annealed samples from PNNL also seems solid, but the determination of it being CoZn intermetallic is less certain. The most compelling evidence is the presence of orientation dependence in the *r*-plane sample. This is well explained by an oriented CoZn model, although the derived distances are not the same as the standard. The orientation dependence implies the CoZn particles are epitaxially constrained by the surrounding ZnO lattice. Such a constraint could explain the changes in bond lengths for the sample deposited on *r*-plane Al_2O_3. The samples on *c*-plane Al_2O_3 did not show an orientation dependence, implying less constraint on the CoZn. However, in this case the contribution to the signal from the short Co-Co distance is small, and the signal is dominated by the Co-Zn bonds. These bonds already have a range of distances in the pure material. The large amplitude of the isolated signal and resulting small Debye-Waller factors in the fits indicate that the spread in distances is reduced for the Co-Zn bonds in the samples as compared to the standard.

There is another possibility that could give a larger bond length than close-packed Co: the formation of particles consisting of an fcc Co:Zn solid solution. This phase is stable at high temperatures up to about 40% Zn and can be quenched to room temperature. Having 12 equidistant near neighbors, it would explain the large amplitude of the isolated metallic signal. However, the largest bond length (for 40% Zn) is 2.57,[42] shorter than necessary to explain our data. Although this could be expanded in this constrained system, expansion did not occur for the similar close-packed Co particles. A fcc Co:Zn solid solution would also not explain the orientation dependence and beating observed for the *r*-plane sample.

The results demonstrate the utility of x-ray absorption measurements in characterizing these types of metal-doped oxide films. Both the XANES and EXAFS are sensitive to the formation of metal bonding to the level of a few percent of the dopant atoms. Both can also be used to determine the amount of any metallic component with similar accuracy. XANES can also verify the valence state of the substitutional atoms, and EXAFS can give a quantitative measurement of the site distortion caused by the substitution.

When the XAFS results are compared to the magnetic properties, some interesting observations can be made. The magnetism cannot be explained by a simple comparison with bulk metal properties. The particle shape and morphology must be playing an important role. In one of the films deposited by the University of Sheffield, S-1, clear evidence for the presence of secondary-phase Co metal particles was observed. This film was not ferromagnetic at room temperature, and the low-temperature study showed that the Co particles were contributing to the hysteretic magnetism observed below 50 K. The most likely conclusion from this study is that the room-temperature magnetism in the other samples from Sheffield is *not* due to the small fraction of metallic particles. We note that the particles with the highest metallic fractions were also the least ferromagnetic. Hence, the ferromagnetism arising directly from the metallic fraction was significantly lower than might be expected, and there is no direct evidence from these samples of a metallic fraction inducing additional oxide ferromagnetism. More on the magnetic properties of these samples will be published elsewhere.

ACKNOWLEDGMENTS

PNC/XOR facilities at the Advanced Photon Source and research at these facilities are supported by the U.S. Department of Energy's office of Basic Energy Sciences, a major facilities access grant from NSERC, Simon Fraser University, and the Advanced Photon Source. Use of the Advanced Photon Source is also supported by the U.S. Department of Energy, Office of Science, Office of Basic Energy Sciences, under Contract No. DE-AC02-06CH11357. Work at Pacific Northwest National Laboratory was performed in the Environmental Molecular Sciences Laboratory, a national scientific user facility sponsored by the Department of Energy's Office of Biological and Environmental Research, and was supported by the U.S. Department of Energy, Office of Science, Office of Basic Energy Sciences, Division of Materials Sciences and Engineering. The Sheffield group would like to acknowledge support from the Engineering and Physical Sciences Research Council for J.R.N., H.J.B., and A.H.B. (studentship), and for experimental facilities.

[1] S. A. Chambers, Surf. Sci. Rep. **61**, 345 (2006).
[2] J. M. D. Coey, Curr. Opin. Solid State Mater. Sci. **10**, 83 (2006).
[3] R. Janisch, P. Gopal, and N. A. Spaldin, J. Phys.: Condens. Matter **17**, R657 (2005).
[4] S. J. Pearton, D. P. Norton, M. P. Ivill, A. F. Hebard, J. M. Zavada, W. M. Chen, and I. A. Buyanova, J. Electron. Mater. **36**, 462 (2007).
[5] S. Deka, R. Pasricha, and P. A. Joy, Phys. Rev. B **74**, 033201 (2006).
[6] T. C. Kaspar, T. Droubay, S. M. Heald, M. H. Engelhard, P. Nachimuthu, and S. A. Chambers, Phys. Rev. B **77**, 201303(R) (2008).
[7] J. H. Park, M. G. Kim, H. M. Jang, S. Ryu, and Y. M. Kim, Appl. Phys. Lett. **84**, 1338 (2004).
[8] K. Rode, R. Mattan, A. Anane, V. Cros, E. Jacquet, J.-P. Contour, F. Petroff, A. Fert, M.-A. Arrio, P. Sainctavit, P. Bencok, F. Wilhelm, N. B. Brookes, and A. Rogalev, Appl. Phys. Lett. **92**, 012509 (2008).
[9] M. Venkatesan, P. Stamenov, L. S. Dorneles, R. D. Gunning, B. Bernoux, and J. M. D. Coey, Appl. Phys. Lett. **90**, 242508 (2007).
[10] A. R. Han, S.-J. Hwang, Y. Zhao, and Y.-U. Kwon, J. Magn. Magn. Mater. **320**, 1591 (2008).
[11] T. C. Kaspar, T. Droubay, Y. Li, S. M. Heald, P. Nachimuthu, C. M. Wang, V. Shutthanandan, C. A. Johnson, D. R. Gamelin, and S. A. Chambers, New J. Phys. **10**, 055010 (2008).

[12] C. Song, K. W. Geng, F. Zeng, X. B. Wang, Y. X. Shen, F. Pan, Y. N. Xie, T. Liu, H. T. Zhou, and Z. Fan, Phys. Rev. B **73**, 024405 (2006).
[13] M. Venkatesan, C. B. Fitzgerald, J. G. Lunney, and J. M. D. Coey, Phys. Rev. Lett. **93**, 177206 (2004).
[14] P. Sati, R. Hayn, R. Kuzian, S. Regnier, S. Schafer, A. Stepanov, C. Morhain, C. Deparis, M. Laugt, M. Goiran, and Z. Golacki, Phys. Rev. Lett. **96**, 017203 (2006).
[15] A. J. Behan, A. Mokhtari, H. J. Blythe, D. Score, X. H. Xu, J. R. Neal, A. M. Fox, and G. A. Gehring, Phys. Rev. Lett. **100**, 047206 (2008).
[16] X. H. Xu, H. J. Blythe, M. Ziese, A. J. Behan, J. R. Neal, A. Mokhtari, R. M. Ibrahim, A. M. Fox, and G. A. Gehring, New J. Phys. **8**, 135 (2006).
[17] X. J. Liu, C. Song, F. Zeng, and F. Pan, J. Phys.: Condens. Matter **19**, 296208 (2007).
[18] F. Pan, C. Song, X. J. Liu, Y. C. Yang, and F. Zeng, Mater. Sci. Eng. R. **62**, 1 (2008).
[19] H.-J. Lee, S. H. Choi, C. R. Cho, H. K. Kim, and S.-Y. Jeong, Europhys. Lett. **72**, 76 (2005).
[20] H. Zhou, L. Chen, V. Malik, C. Knies, D. M. Hofmann, K. P. Bhatti, S. Chaudhary, P. J. Klar, W. Heimbrodt, C. Klingshirn, and H. Kalt, Phys. Status Solidi A **204**, 112 (2007).
[21] J. D. Bryan, S. M. Heald, S. A. Chambers, and D. R. Gamelin, J. Am. Chem. Soc. **126**, 11640 (2004).
[22] S. A. Chambers, S. M. Heald, and T. Droubay, Phys. Rev. B **67**, 100401(R) (2003).
[23] K. A. Griffin, A. B. Pakhomov, C. M. Wang, S. M. Heald, and K. M. Krishnan, Phys. Rev. Lett. **94**, 157204 (2005).
[24] D. H. Kim, J. S. Yang, Y. S. Kim, T. W. Noh, S. D. Bu, S.-I. Baik, Y.-W. Kim, Y. D. Park, S. J. Pearton, J.-Y. Kim, J.-H. Park, H.-J. Lin, C. T. Chen, and Y. J. Song, Phys. Rev. B **71**, 014440 (2005).
[25] G. Martínez-Criado, A. Segura, J. A. Sans, A. Homs, J. Pellicer-Porres, and J. Susini, Appl. Phys. Lett. **89**, 061906 (2006).
[26] M. Murakami, Y. Matsumoto, T. Hasegawa, P. Ahmet, K. Nakajima, T. Chikyow, H. Ofuchi, I. Nakai, and H. Koinuma, J. Appl. Phys. **95**, 5330 (2004).
[27] S. M. Heald, E. A. Stern, D. Brewe, R. A. Gordon, E. D. Crozier, D. Jiang, and J. O. Cross, J. Synchrotron Radiat. **8**, 342 (2001).
[28] S. Kraft, J. Stumpel, P. Becker, and U. Kuetgens, Rev. Sci. Instrum. **67**, 681 (1996).
[29] T. Hori, H. Shiraish, and Y. Ishii, J. Magn. Magn. Mater. **310**, 1820 (2007).
[30] T. J. Prior, D. Nguyen-Manh, V. J. Couper, and P. D. Battle, J. Phys.: Condens. Matter **16**, 2273 (2004).
[31] C. B. Shoemaker, D. P. Shoemaker, T. E. Hopkins, and S. Yindepit, Acta Crystallogr., Sect. B: Struct. Crystallogr. Cryst. Chem. **34**, 3573 (1978).
[32] CoZn powder synthesized at the Materials Preparation Laboratory, Ames Laboratory, US DOE (see www.mps.ameslab.gov).
[33] B. Ravel and M. Newville, J. Synchrotron Radiat. **12**, 537 (2005).
[34] A. L. Ankudinov, A. I. Nesvizhskii, and J. J. Rehr, Phys. Rev. B **67**, 115120 (2003).
[35] S. M. Heald and E. A. Stern, Phys. Rev. B **16**, 5549 (1977).
[36] S. Zhou, K. Potzger, J. von Borany, R. Grötzschel, W. Skorupa, M. Helm, and J. Fassbender, Phys. Rev. B **77**, 035209 (2008).
[37] D. A. Schwartz, N. S. Norberg, Q. P. Nguyen, J. M. Parker, and D. R. Gamelin, J. Am. Chem. Soc. **125**, 13205 (2003).
[38] J. R. Neal, A. J. Behan, R. M. Ibrahim, H. J. Blythe, M. Ziese, A. M. Fox, and G. A. Gehring, Phys. Rev. Lett. **96**, 197208 (2006).
[39] F. W. Kampers, C. W. R. Engelen, J. H. C. v. Hooff, and D. C. Koningsberger, J. Phys. Chem. **94**, 8574 (1990).
[40] K. I. Pandya, S. M. Heald, J. A. Hriljac, L. Petrakis, and J. Fraissard, J. Phys. Chem. **100**, 5070 (1996).
[41] R. B. Greegor and F. W. Lytle, J. Catal. **63**, 476 (1980).
[42] J. Schramm, Z. Metallkd. **33**, 46 (1941).
[43] A. Ney, P. Poulopoulos, and K. Baberschke, Europhys. Lett. **54**, 820 (2001).